A&A 417, 107–114 (2004)
DOI: 10.1051/0004-6361:20031775

Astronomy & Astrophysics

CO observations in the direction of southern HII regions⋆,⋆⋆

D. Russeil[1] and A. Castets[2,3]

[1] Laboratoire d'Astronomie de Marseille, 2 place Le Verrier, 13248 Marseille Cedex 04, France
[2] Laboratoire d'Astrophysique de l'Observatoire de Grenoble, BP 53, 38041 Grenoble Cedex 9, France
[3] Observatoire de Bordeaux, 2 rue de l'Observatoire, 33270 Floirac, France

Received 4 August 2000/ Accepted 2 December 2003

Abstract. We present ^{12}CO(1–0), ^{12}CO(2–1) and/or ^{13}CO(1–0) observations, obtained with the 15 m SEST telescope, in the direction of 252 southern HII regions located within 2° of the galactic plane and in the interval 280° $< l <$ 355°. The data presented here are an important contribution to the study of the large scale structure of our Galaxy (not discussed here) as molecular information is part of the multi-wavelength study of the galactic plane. We used kinematical criteria to distinguish between lines associated with HII regions and non-associated ones. We find that HII regions are associated with molecular lines exhibiting a line-width larger than 2.5 km s^{-1}. From a kinematical point of view we find that the velocity difference (Vco-VHII) peaks at 0 km s^{-1}. Non-associated CO lines with the same kinematics as diffuse Hα emission (the Warm Interstellar Medium) are used to extract some statistical properties encountered in this more diffuse medium. We can determine the velocity of the three diffuse ionised gas layers detected in Hα: −3.6, −26.5 and −45.5 km s^{-1}.

Key words. ISM: molecules – ISM: HII regions – ISM: clouds

1. Introduction

Despite strong observational efforts over the past thirty years, the spiral pattern of our galaxy is still not determined exactly. However, as the star-forming complexes are known to be good tracers of the spiral arms of galaxies, it is possible to trace this pattern, provided we can dearly identify these giant star-forming complexes and obtain a precise determination of their systemic velocity to compute their distance.

These star-forming complexes are made up of molecular gas and HII regions with their exciting stars surrounded by diffuse ionised hydrogen. Clear identification of such a complex requires one to gather these various objects into one single physical group taking into account their intrinsic spatial and velocity dispersion. As a first approximation, we can associate HII region with molecular clouds having identical radial velocity. But the physical link between molecular and ionised gas may not be obvious: the ionised gas can exhibit large internal motions and/or intricate velocity fields. For instance when an HII region bursts out of the molecular cloud edges by the "champagne effect", the velocity of the ejected gas may reach 10 km s^{-1} with respect to the cloud and to the stationary parts of the ionised region (Tenorio-Tagle 1979). Such a velocity departure leads to an erroneous systemic velocity determination and therefore an erroneous derived kinematic distance (Marcelin et al. 1994; Russeil et al. 1995, and references therein). In addition, the coupling of the molecular and HII region optical emission helps us to solve the well-known distance ambiguity problem of the complexes situated inside the solar circle: the Hα counterpart to the molecular gas suggests that we rather choose the nearest kinematical distance (e.g. Georgelin et al. 2000, 1996). Also, HII region velocities provide a crucial link between star distances and molecular cloud velocities.

Therefore, the knowledge of the velocity of the molecular and ionised gas towards HII regions is imperative to delineate star-forming complexes and to correct their kinematic distance for champagne and other effects. It is in this framework that a southern galactic plane Hα survey (thereafter noted MHS, for Marseille Hα Survey), about to be completed, was conducted at La Silla, ESO. Equipped with a scanning Fabry-Perot interferometer, the instrument give the Hα profile, hence kinematic information of the ionised gas, over 38′ × 38′ fields with a 9″ × 9″ spatial resolution (le Coarer et al. 1992).

A CO survey of the southern Milky Way at low resolution (8.8 arcmin) has already been performed by Bronfman et al. (1989). The spatial resolution of these observations are very far from our 9″ Hα observations. Only a few regions have been observed in CO at high resolution (e.g. Gillespie et al. 1977,

Send offprint requests to: D. Russeil,
e-mail: delphine.russeil@oamp.fr

⋆ Based on observations collected at the European Southern Observatory.

⋆⋆ Tables 2 and 3 are only available in electronic form at the CDS via anonymous ftp to cdsarc.u-strasbg.fr (130.79.128.5) or via http://cdsweb.u-strasbg.fr/cgi-bin/qcat?J/A+A/417/107

1979; de Graauw et al. 1981; Israel et al. 1984; Phillips et al. 1986; Zinchenko et al. 1995). Low spatial resolution surveys are extremely useful to determine the molecular cloud extension and global velocity dispersion while high resolution is necessary to establish a clear relationship between molecular and ionised gas velocities. The SEST telescope is perfectly suited for such molecular studies since its beamwidth is closer to the spatial resolution of our Hα maps. We used this instrument to measure molecular velocities towards HII regions in the southern hemisphere which have never been observed at millimeter wavelengths.

2. Observations and data reduction

The analysis presented in this paper is based on observations made in July 1996 and 1997 with the 15-m SEST radiotelescope located in La Silla, Chile. The sample consists of 252 HII regions. During the first run only one receiver was available, hence only the ^{13}CO(1–0) line was observed. A detailed description of the characteristics of the SEST telescope is given in Booth et al. (1989). The single sideband system temperature (including sky and forward efficiency corrections) of the dual SIS receiver varied from 120 to 250 K for the 2.6 mm receiver and from 315 to 390 K for the 1.3 mm receiver depending on weather conditions and elevation. To get the maximum velocity resolution we used the narrow high-resolution acousto-optical spectrometer equipped with a 2048 pixel linear CCD giving a sampling of 43 kHz. The velocity resolution is 0.12 and 0.06 km s^{-1} at 2.6 mm and 1.3 mm respectively. The SIS receiver was calibrated by inserting two different temperature loads. The sky opacity was estimated regularly using the usual chopper-wheel technique. The weather was always stable and clear during the observations; therefore the opacity of the ^{12}CO(1–0) and ^{13}CO(1–0) lines was never higher than 0.2 and 0.12 respectively, while the opacity of the ^{12}CO(2–1) line never exceeded 0.3. All data were obtained using either the frequency switching mode (frequency throw of 20 MHz) or the position switching mode depending on the extension of components seen in the spectrum. The position switching mode was systematically used in all directions close to the galactic center. All OFF positions were carefully checked, using the frequency switched mode, to be emission free. All OFF positions used are listed in Table 1. The mean integration times were 2 min per source which resulted in an rms noise equal to 72 mK in ^{13}CO(1–0), 140 mK in ^{12}CO(1–0) and 40 mK in ^{12}CO(2–1). The beamwidth of the telescope is equal to 42″ and 21″ at 115 and 230 GHz respectively. The pointing accuracy which was checked every two hours on the Orion SiO maser was found to be better than 4″. All intensities quoted in this paper are given in main beam temperature $T^*_{\rm mb}$ (i.e. are corrected for antenna main beam efficiency).

All observed sources belong to the fourth galactic quadrant; they are situated either in the Sagittarius arm or into the Scutum-Crux and Norma inner arms. All sources were selected from the Marseille Hα survey and radio continuum surveys (Haynes et al. 1978; Caswell & Haynes 1987). They correspond to 5 GHz continuum sources and Hα HII regions with no known CO counterpart.

Table 1. The OFF positions.

l(°)	290	300	303.3	309	320	326	326	330.5
b(°)	3	3	3.3	−4	−3.6	−3	−4	4
l(°)	333	334	334	343	344	345	347	347
b(°)	−3	2	3	4	3	4	−3	−5

3. Results

3.1. CO line – HII region association

95% of observed sources are detected in ^{12}CO, 88% of them showing ^{12}CO(1–0) detection while in ^{13}CO(1–0) 85% of sources show detection. Morphologically, the spectral lines appear symmetric, multipeaked, winged or flat topped (some representative examples are given in Fig. 1). Such non-Gaussian features are usually attributed to ejection, accretion, rotation, self absorption, saturation or the superposition of several lines along the line of sight. The distinction between the intrinsic and extrinsic profile distortions is difficult and would require a mapping method. For example intrinsic self-absorption and self-absorption due to the presence of a "cold" cloud lying somewhere in the line of sigth (e.g. Phillips et al. 1981) give similar observed profiles.

To analyse the spectra we performed a multi-Gaussian decomposition (as done by e.g. Otrupcek et al. 2000); i.e. lines with wings or multiple peaks were fitted with several Gaussians. The parameters of the fits are given in Tables 2 and 3. The uncertainty on the velocity determination is 0.2 km s^{-1}. Nearly all the observed spectra exhibit several lines. Among these lines one can assume that only one is associated with the HII region, the other ones being emitted by other starless molecular clouds in the same line of sight.

To associate the CO line with an HII region we follow the method of Whiteoak et al. (1982): we plot the distribution of CO line peak temperature as a function of the velocity difference between CO and recombination lines (Fig. 2). In this plot a discontinuity is found at a velocity of about 10 km s^{-1} (width at half height of the main peak in Fig. 2 bottom) suggesting that there is association when the velocity difference is less than or equal to 10 km s^{-1} (Avedisova 1997 gives the association for velocity difference $\leq$7 km s^{-1}). Whiteoak et al. (1982) found the discontinuity at 5 km s^{-1}. What can explain such a difference? It has been demonstrated (Tenorio-Tagle 1979, 1982; Yorke 1986) that HII regions in some cases may exhibit a "champagne flow" corresponding to a supersonic expansion of the ionised gas toward the inter-cloud medium. In such a case the velocity of the ionised gas respective to the molecular cloud may exceed 10 km s^{-1}. A good example is the Orion nebula (e.g. Castets et al. 1990): the associated molecular cloud has a velocity of 9 km s^{-1} while the HII region exhibits a velocity of −5 km s^{-1}. This is interpreted as the expansion of the ionised gas towards us with a velocity of ∼14 km s^{-1}. Another example can be seen in Fig. 8: G305.678+1.607 has a velocity falling in the wing of the clearly associated CO line. Indeed, only one isolated CO cloud at −52 km s^{-1} on Bronfman's et al. (1989) CO maps is detected, making the association

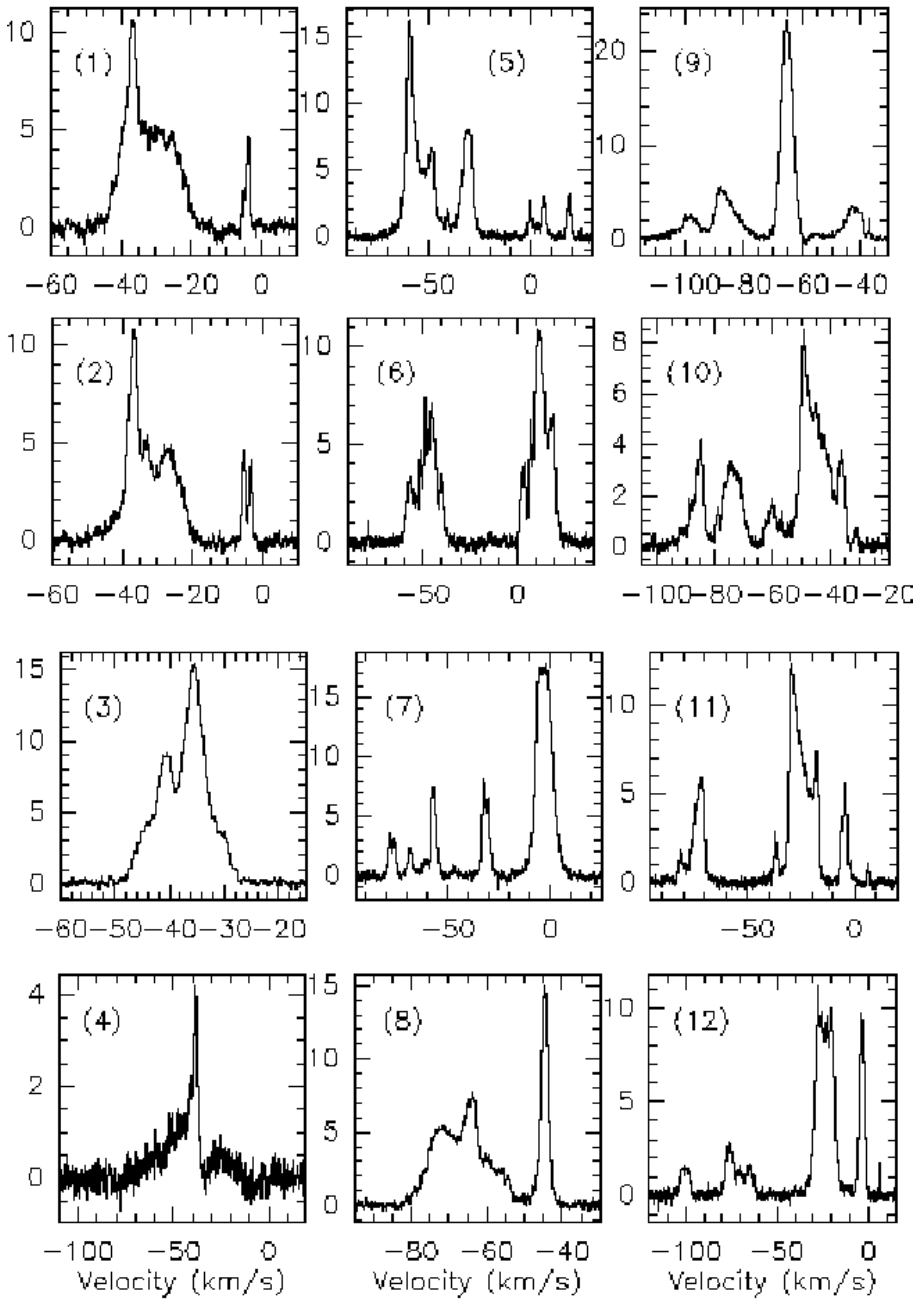

Fig. 1. Sample of ^{12}CO(1–0) line profiles (Tmb (K) versus Vlsr (km s^{-1})): (1): G305.0+0.1, (2): G305.1+0.1, (3): G305.8-0.0, (4): G308.6+0.5, (5): G311.4+0.3, (6): G315.3-0.2, (7): G320.3+0.1, (8): G328.0-0.5, (9): G331.3-0.3, (10): G332.9+0.7, (11): G343.9-0.6 and (12): G344.2-0.5.

unambiguous. Hence, we have a molecular-HII region velocity difference of ∼9 km s^{-1}. In parallel, the mean cloud-cloud dispersion velocity being between 3 and 9 km s^{-1} (Liszt et al. 1984; Stark 1984; Stark & Brand 1989) we can expect that lines separated by more than this quantity probably belong to different complexes. Then we can adopt a velocity difference <10 km s^{-1} as a kinematic criterion for an association.

Using this criterion we find that in 81% of the ^{12}CO observations and in 77% of the ^{13}CO ones a molecular line is clearly associated with an HII region. Most certainly, some of the non-detections can be attributed to a displacement in projection on the plane of the sky of the molecular cloud from the brightest part of the HII region. Only in 5% of the ^{12}CO observations does the ionised gas velocity fall between two CO peaks making difficult the choice of the associated peak. In this case a direct association is difficult, hence, we made use of additional information such as multiwavelength and large-scale information to determine the association.

In Figs. 3 and 4 the non-associated lines show a clear tendency to be faint and narrow while HII regions are more preferentialy but not systematically associated with intense lines.

To prove such tendency we have plotted (Fig. 5) CO peak intensities versus line widths. Clemens & Barvainis (1988) and Clemens et al. (1991) distinguish 4 parts (solid lines in Fig. 4):

– the lower left corner: mainly populated by Bok globules and quiescent clouds;

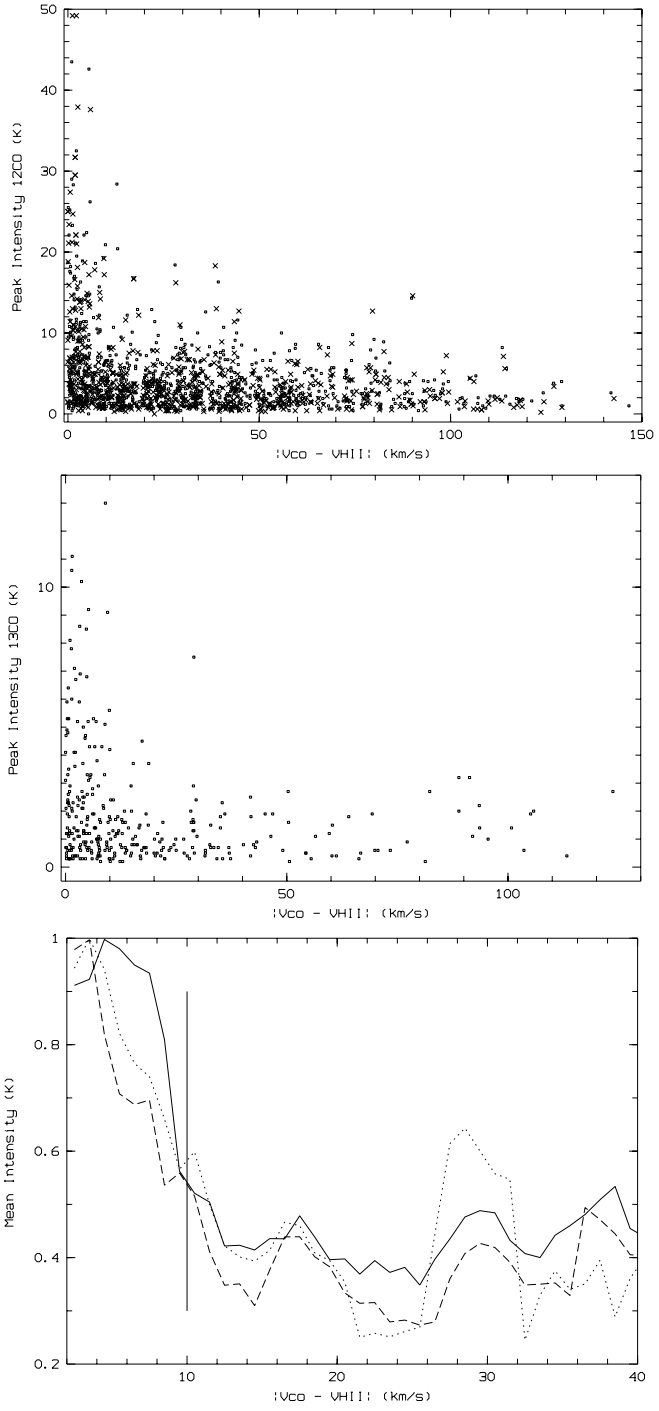

Fig. 2. *Up*: peak intensity versus absolute value of molecular-ionised gas velocity difference (squares: ^{12}CO(1–0), crosses: ^{12}CO(2–1)). *Middle*: same as above but for ^{13}CO(1–0). *Bottom*: mean peak intensity runnind window normalized plots (size = 5 km s^{-1}, step = 2 km s^{-1}). The doted, full and dashed lines correspond respectively to ^{13}CO(1–0), ^{12}CO(1–0) and ^{12}CO(2–1). The vertical line indicates the 10 km s^{-1} position.

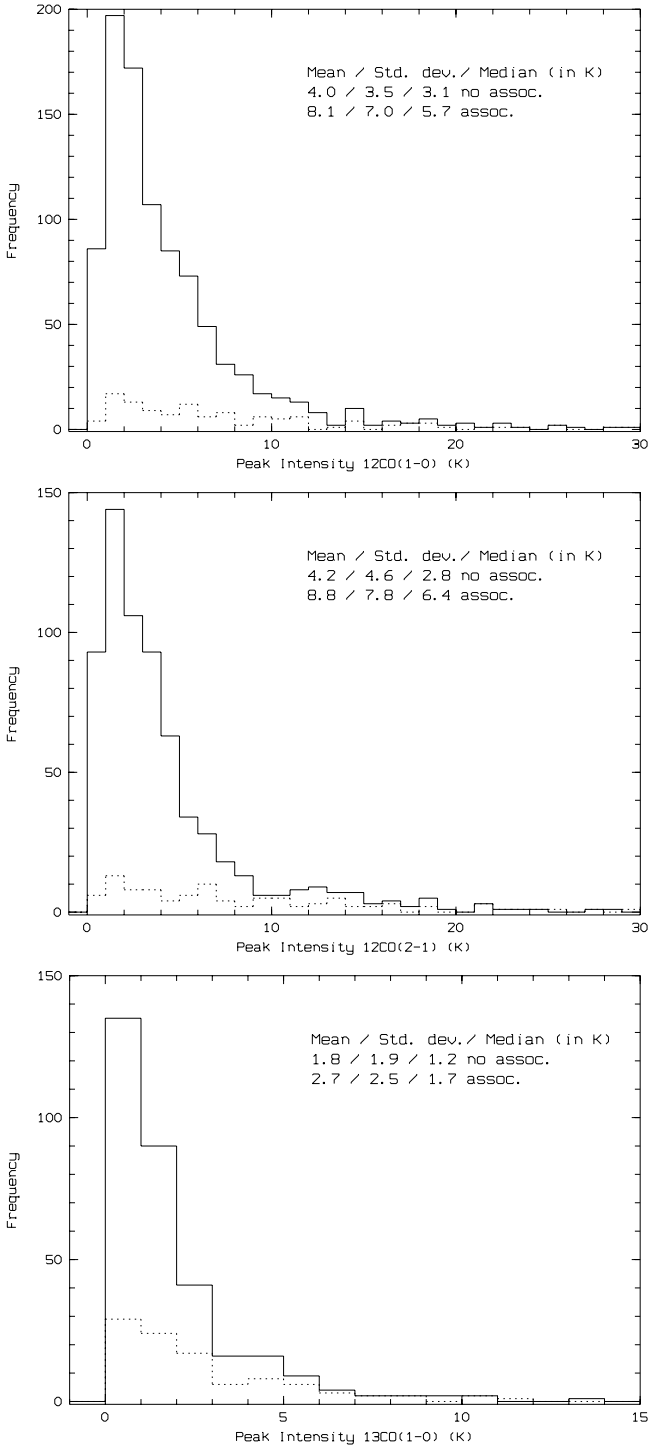

Fig. 3. Peak intensity histogram for line associated (dashed line) or not (full line) with HII region. Mean and median values are indicated on each panel.

– the upper left corner: expected location for clouds with unusual warm temperatures but narrow lines, corresponding probably to gas heated by non-embedded local radiation;
– the lower right corner: lines are quite broad implying dynamical activity but cool gas temperatures. It is the expected location for clouds with embedded star-formation activity;
– the upper right corner: expected location for hot dynamically active clouds associated with HII regions.

This plot confirms the tendency underlined by histograms. Since most of lines reside in the two right corners, they are likely to be associated with active clouds. More precisely 58% of lines associated with HII region (42% in the upper right) and 85% of non-associated lines (8.4% being in the lower left

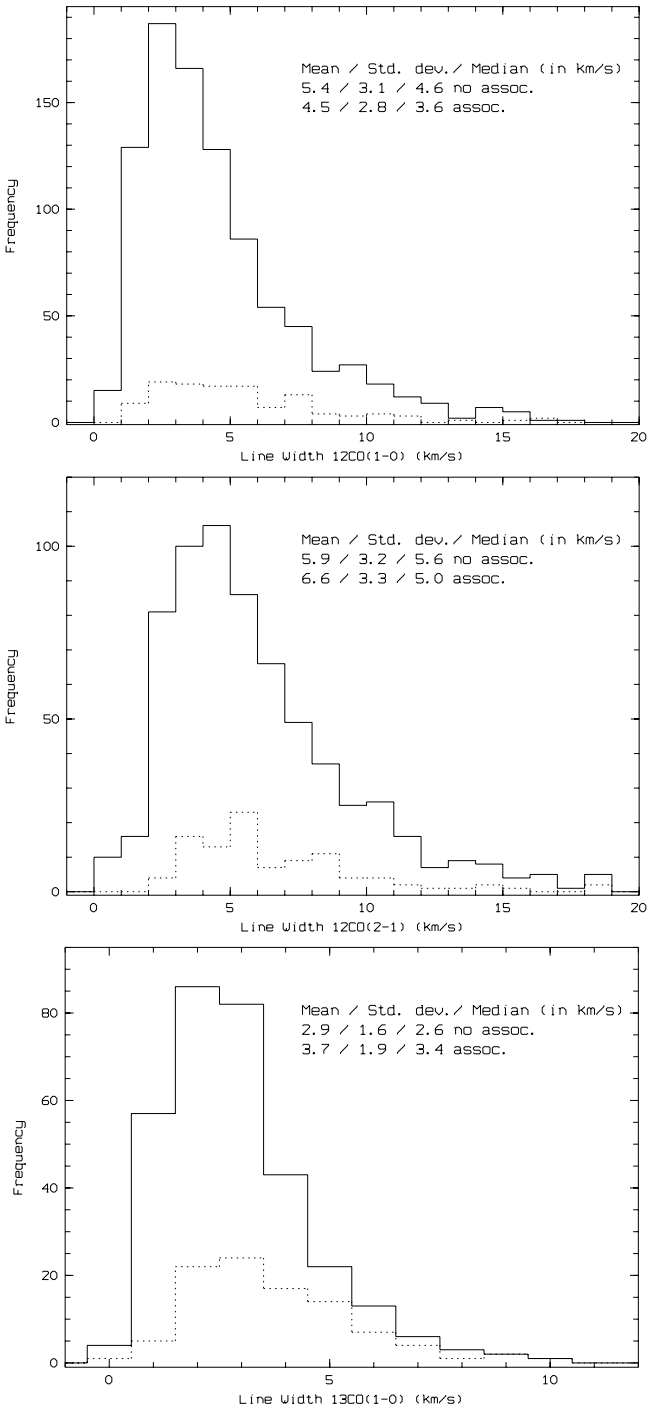

Fig. 4. Line width histogram for line associated (dashed line) or not (full line) with HII region. Mean and median values are indicated on each panel.

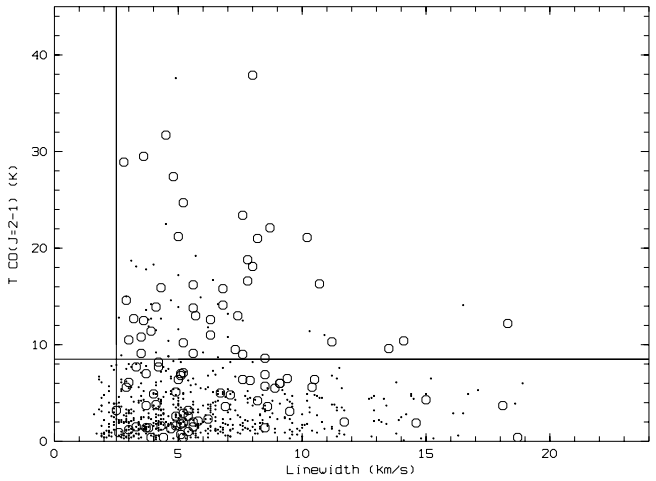

Fig. 5. Distribution of CO temperature versus line widths. Open circles and points indicate respectively line associated or not with HII region. The solid lines at 2.5 km s^{-1} and 8.5 K divide the diagram into 4 quadrants as in Clemens & Barvainis (1988).

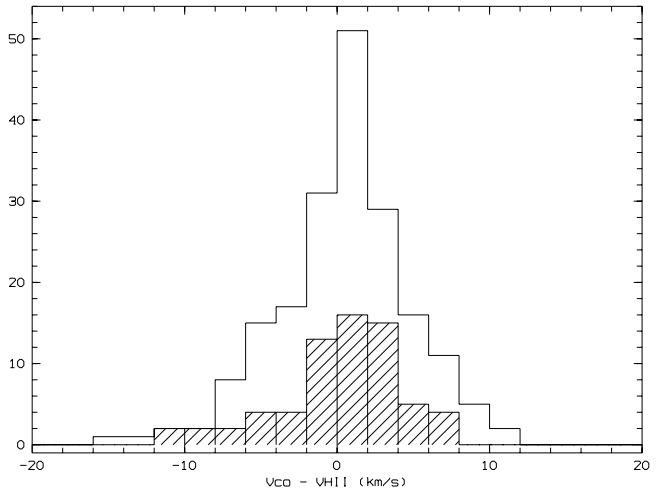

Fig. 6. Molecular-ionised gas velocity difference distribution. Empty histogram: all HII regions (191 objects, mean: -0.018 ± 0.1 km s^{-1}, standard deviation: 4.30 km s^{-1}). Hashed histogram: optically detected HII regions (68 objects, mean: 0.016 ± 0.2 km s^{-1}, standard deviation: 4.84 km s^{-1}).

corner, and 6.6% in the upper right corner) reside in the lower right corner.

The distribution of the lines associated with HII regions can be related to the evolutionary stage: we can suspect that during its evolution from a young compact stage through a "champagne" phase to an old extended and diffuse stage (where the molecular material can be destroyed by the ionising and dissociation radiations from the exciting stars and blown away by the stellar wind), an HII region and its exciting star(s) interact differently with its parental molecular cloud leading its associated CO line parameters to move up through the right corners. But, it is not possible, without mapping, to go deeper in the CO line interpretation as it depends strongly on the cloud geometry, clumpiness, density, UV illumination ... Indeed, for example, Williams et al. (1995) note for M 17 a higher CO brightness temperature closer to the center of the HII region while Schneider et al. (1998) observes a steep decline of the molecular emission towards the center of the Rosette HII region.

Concerning the lines which are not associated with HII regions, their bulge distribution in the lower right corner suggests that there are some warm clouds which probably participate in the spiral arms pattern. A few lines are located in the lower left corner, all of them being not associated with HII region. This is not surprising since this corner is mainly populated by Bok globules, dark clouds and small quiescent molecular clouds

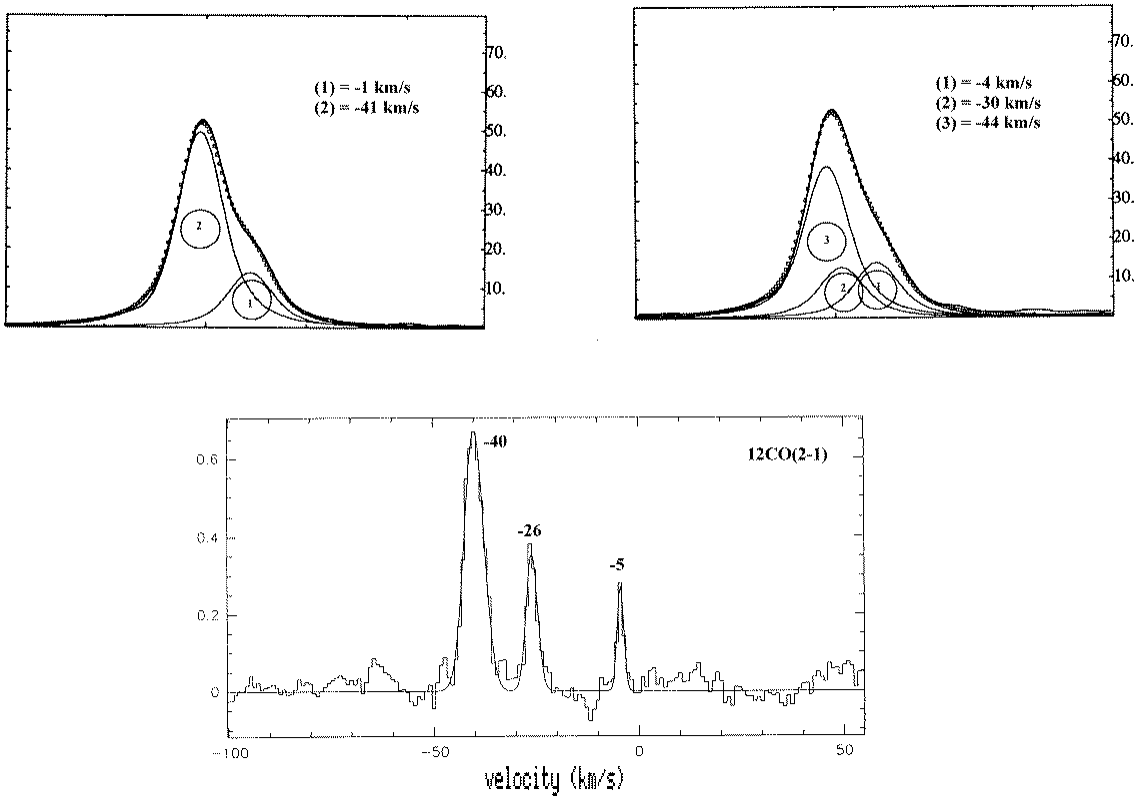

Fig. 7. Hα and CO profiles for the source G301.8+1.0 (=G301.814+1.077, Caswell & Haynes 1987). The Hα profile decomposition with 2 or 3 components is equiprobable. The CO profile rather supports the 3-components decomposition.

(Clemens & Barvainis 1988; Clemens et al. 1991; Otrupeck et al. 2000). We note that the upper left corner is not populated at all.

3.2. Velocity distribution

Figure 6 shows the distribution of the velocity difference between molecular and ionised gas. The uncertainty on the molecular velocity is ∼0.2 km s^{-1} (deduced from the line fitting uncertainties), the uncertainty on the Hα velocity is 1 km s^{-1} (Le Coarer et al. 1992) and the uncertainty on the radio recombinaison velocity is ∼1 km s^{-1} (Caswell & Haynes 1987). Hence we can adopt 1.5 km s^{-1} as the uncertainty on the velocity difference.

The HII region histogram (Fig. 6) gives a mean value for the velocity difference close to 0 km s^{-1}, a result already obtained by Myers et al. (1986) and Waller et al. (1987). This indicates that the ionised gas expands randomly with respect to the molecular gas. If we look at the optical HII region only, we note that the mean velocity difference is ∼0 km s^{-1}. In the past, a positive but small value was observed by Fich et al. (1990) (<Vco-VHII> = 1.5 km s^{-1}, from 284 regions), Deharveng (1980) (<Vco-VHII> = 2.3 km s^{-1} from 65 regions) and Israel (1978) (<Vco-VHII> = 3.4 km s^{-1} from 50 regions). A positive difference is expected if optically visible regions are supposedly located on the near side of their molecular cloud, hence with an ejection of matter preferentially towards us (Israel 1978). Our value of <Vco-VHII> supports the unobscured models of Fich et al. (1990). In this way the optical observational sensitivity limitation can play a role. Indeed, the mean velocity difference found by the above authors, decreases with the number of regions taken into account and the date of publication. We might suspect a selection effect due to the fact that in the past the optically observed HII regions were the brightest and evolved ones. Now thanks to higher instrumental performance, fainter and more compact HII regions are detected in the optical range. This could explain the convergence of the peak distribution to 0 km s^{-1} as our sample excludes such bright and evolved regions.

3.3. Comparison CO – Hα profiles

The molecular profiles can be compared with the Hα ones obtained with the MHS. In such Hα profiles several ionised hydrogen emissions superimposed on the line of sight are always resolved: in addition to the discrete HII region emissions, diffuse emission, associated with the Warm Interstellar Medium (e.g. Sivan 1986; Reynolds 1990), are dectected. But the identification of the individual components is made difficult by the intrinsic width of the line (typical thermal line width 25 km s^{-1}). The narrower CO spectra provide information required to perform the multi-Gaussian fit of the Hα profiles by keeping the center velocities fixed to CO values. This approach has been used in Georgelin et al. (2000) and is here illustrated in Fig. 7.

In addition the comparison of Hα and CO profiles can provide information on the diffuse ionised gas. For example, the case of the source G305.678+1.607. Three Hα components

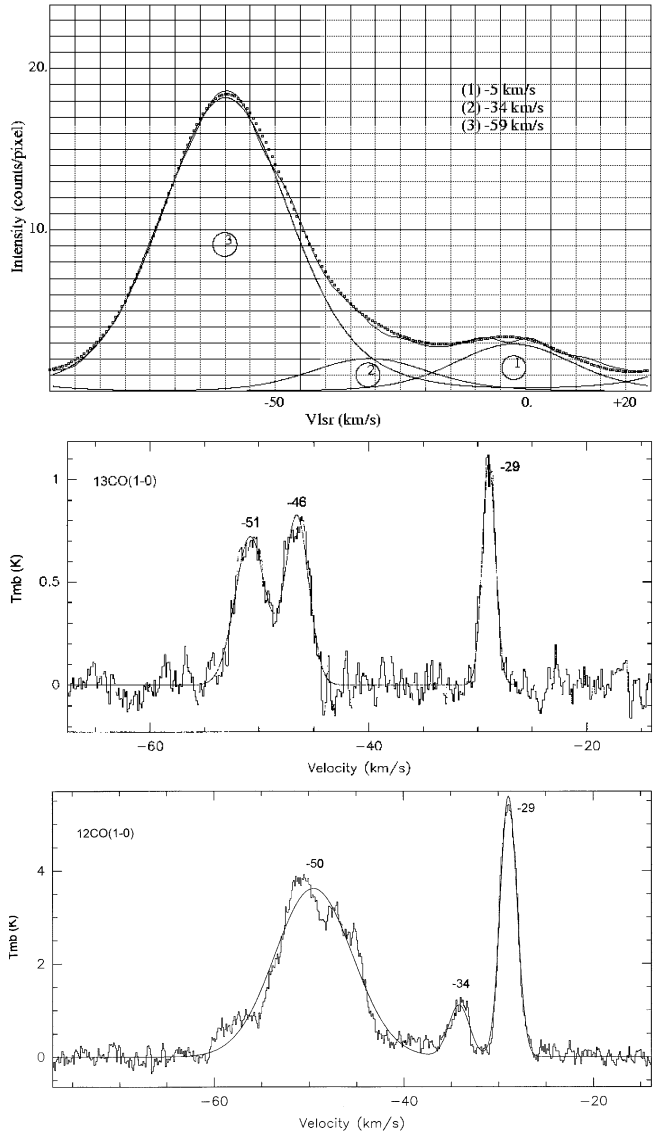

Fig. 8. Hα and CO profiles for the source G305.6+1.6 (=G305.678+1.607, Caswell & Haynes 1987). In this case, the Hα decomposition is unambiguous.

are well identified (Fig. 8) at −5, −34 and −59 km s^{-1}. The −59 km s^{-1} component is emited by the HII region G305.678+1.607 while the two others are diffuse emissions present in the line of sight: the −5 km s^{-1} corresponds to a local diffuse emission while the −34 km s^{-1} is a diffuse emission located in the Carina arm (Russeil et al. 1998). Compared to the CO profile, the HII region can be associated with the molecular line with a mean ^{12}CO(1–0) velocity at −50 km s^{-1}. We have a molecular line at the same velocity as the −34 km s^{-1} diffuse emission while no CO is found associated with the local one. Conversely, no Hα counterpart is detected for the −29 km s^{-1} molecular line.

If CO and diffuse Hα coincide kinematically nothing here provides information about their physical link. This is not surprising since molecular clouds are expected to be distributed preferentialy along the arms (e.g. Grabelsky et al. 1987) following the same kinematics. However, the fact that the CO counterpart to diffuse Hα is not systematic suggests that

Table 4. Mean line parameters of CO lines falling in diffuse Hα emission velocity ranges.

	^{12}CO(1–0)	^{12}CO(2–1)	^{13}CO(1–0)
Compo. 1.			
% of line	25.8	27.4	26.1
Vel. (km s^{-1})	−3.6 ± 4.4	−3.1 ± 4.7	−4.1 ± 4.5
Width (km s^{-1})	3.3 ± 2.8	4.9 ± 4.3	1.8 ± 1.1
Int. (K)	3.6 ± 3.5	3.4 ± 3.2	1.0 ± 0.9
Compo. 2.			
% of line	35.5	34.4	22.4
Vel. (km s^{-1})	−26 ± 5.4	−25.9 ± 5.4	−27.3 ± 5.1
Width(km s^{-1})	3.8 ± 2.3	5.1 ± 3.1	2.9 ± 1.8
Int. (K)	4.2 ± 3.9	3.9 ± 4.8	1.5 ± 1.4
Compo. 3.			
% of line	38.7	38.3	51.5
Vel. (km s^{-1})	−45.6 ± 4.9	−45.5 ± 5.1	−45.0 ± 5.0
Width (km s^{-1})	4.8 ± 3.1	6.6 ± 3.9	3.0 ± 1.6
Int. (K)	5.1 ± 3.9	4.9 ± 3.8	2.0 ± 2.2

Hα emission is widespread and can reside in areas where CO density is low. Indeed, in Hα, the diffuse components are detected whatever the observed directions. Especially, three diffuse layers are always detected in the fourth galactic quadrant with velocity ranges (e.g. Georgelin et al. 1994, 1996, 2000; Russeil 1997; Russeil et al. 1998): (1) +6 to −12 km s^{-1} (local component); (2) −17 to −35 km s^{-1} (Saggitarius-Carina arm); (3) −37 to −52 km s^{-1} (Scutum-Crux arm). These velocity ranges delimit the main local spiral features and we can search for possible properties of the non-associated CO lines falling in these velocity ranges (see Table 4). We note a similar detection rate in ^{12}CO for components 2 and 3 while more than half of the ^{13}CO(1–0) detections are in the third component velocity range. This suggests that ^{13}CO(1–0) appears preferentialy located in the Scutum-Crux arm while ^{12}CO is similarly distributed in the Carina and Scutum-Crux spiral arms. As ^{13}CO traces denser parts of clouds than ^{12}CO, this can suggest that denser clouds are located in the Scutum-Crux arm. We note also a slight increase of the peak temperature from the local component to the farthest one which could reflect an increase of the excitation temperature from the outer to inner Galaxy (Mead & Kutner 1988).

However, this analysis is limited by the non-completness of our CO sample, and by the necessity a detailled comparison between CO and Hα spectra source by source.

4. Conclusion

We report a catalogue of CO observations towards 252 HII regions situated in the southern galactic plane. These observations are to be included in a multi-wavelength study of the

plane of our Galaxy (see Russeil 1998, 2003). We illustrated how the CO information can be compared with the Hα and we performed a statistical analysis. From a comparison of the molecular cloud and ionised gas emission we were able to associate more than 81% of the observed molecular lines with HII regions. The remaining lines that are not clearly associated with discrete HII regions are probably clouds with embedded star formation. The large sample of directions observed can provide a framework for further, more detailed, physical and kinematical study of the interaction between HII regions and molecular clouds.

References

Avedisova, V. S. 1997, Ap&SS, 252, 261
Booth, R. S., Delgado, G., Hagstrom, M., et al. 1989, A&A, 216, 315
Bronfman, L., Alvarez, H., Cohen, R. S., & Thaddeus, P. 1989, ApJS, 71,481
Castets, A., Duvert, G., Dutrey, A., et al. 1990, A&A, 234, 469
Caswell, J. L., & Haynes, R. F. 1987, A&A, 171, 261
Clemens, D. P., & Barvainis, R. 1988, ApJ, 68, 257
Clemens, D. P., Yun, J. L., & Heyer, M. H. 1991, ApJS, 75, 877
le Coarer, E., Amram, P., Boulesteix, J., et al. 1992, A&A, 257, 389
Deharveng, L. 1980, Ph.D. Thesis, Université de Provence
Fich, M., Treffers, R. R., & Dahl, G. P. 1990, AJ, 99, 622
Gieriens, K. M., Stutzhi, J., & Winnerwisser, G. 1992, A&A, 259, 271
Gillespie, A. R., Huggins, P. J., Sollner, T. C. L. G., et al. 1977, A&A, 60, 221
Gillespie, A. R., White, G. J. & Watt, G. D. 1979, MNRAS, 186, 383
Georgelin, Y. M., Russeil, D., Marcelin, M., et al. 1996, A&AS, 120, 41
Georgelin, Y. M., Russeil, D., Amram, P., et al. 2000, A&A, 357, 308
de Graauw, T., Lidholms, S., Fitton, B., et al. 1981, A&A, 102, 257
Hasegawa, T. 1997, CO: Twenty Five years of millimetric-wave Spectroscopy, ed. W. B. Latter, S. J. E. Radford, P. R. Jewell, J. G. Mungun, & J. Bally (Dordrecht: Kluwer), 39
Haynes, R. F., Caswell, J. L., & Simons, L. W. J. 1978, Aust. J. Phys. Astrophys. Suppl., 45, 1
Israel, F. P. 1978, A&A, 70, 769
Liszt, H. S., Burton, W. B., & Xiang, D. L. 1984, A&A, 140, 303
Marcelin, M., Georgelin, Y. M., Amram, P., & Georgelin, Y. P. 1995, IAU Coll., 149, ASP Conf. Ser., 71, 160
Mead, K. N., & Kutner, M. L. 1988, ApJ, 330, 399
Myers, P. C., Dame, T. M., Thaddeus, P., et al. 1986, ApJ, 301, 398
Phillips, J. P., de Vries, C. P., & de Grauuw, T. 1986, A&AS, 65, 465
Phillips, J. P., Knapp, G. R., Huggins, P. J., et al. 1981, ApJ, 245, 512
Russeil, D., Georgelin, Y. M., Georgelin, Y. P., et al. 1995, A&AS, 114, 1
Russeil, D. 1998, Ph.D. Thesis, Université de Provence
Russeil, D., Georgelin, Y. M., Amram, P., et al. 1998, A&A, 130, 119
Russeil, D. 2003, A&A, 397, 133
Sakamoto, S., Hayashi, M., Hasegawa, T., Handa, T., & Oka, T. 1994, ApJ, 425, 641
Sakamoto, S., Hayashi, M., Hasegawa, T., Handa, T., & Oka, T. 1996, in Unsolved problems of the MW, 501, ed. Blitz & Teuben
Schneider, N., Stutzki, J., Winnewisser, G., & Block, D. 1998, A&A, 335, 1049
Solomon, P. M., Rivolo, A. R., Barrett, J., & Yahil, A. 1987, ApJ, 319, 730
Stark, A. A. 1984, ApJ, 281, 624
Stark, A. A., & Brand, J. 1989, ApJ, 339, 763
Tenorio-Tagle 1979, A&A, 71, 59
Tenorio-Tagle 1982, in Regions of recent star formation, ed. Roger, et al.
Waller, W. H., Clemens, D. P., Sanders, D. B., & Scoville, N. 1987, ApJ, 314, 397
Whiteoak, J. B., Robina, E. O., & Rennie, C. J. 1982, Proc. ASA, 4, 434
Williams, J. P., Blitz, L., & Stark, A. A. 1995, ApJ, 451, 252
Yorke, H. W. 1986, ARA&A, 24, 49
Zinchenko, I., Mattila, K., & Toriseva, M. 1995, A&AS, 111, 95